Global Oceans 2020: Singapore - U.S. Gulf Coast

Differential Ultrasonic Detection of Small Objects for Underwater Applications

Fabian John*, Roman Kusche*, Felix Adam* and Horst Hellbrück*
* Technische Hochschule Lübeck, Germany
Department of Electrical Engineering and Computer Science, Center of Excellence CoSA
Email: fabian.john, roman.kusche, felix.adam, horst.hellbrueck@th-luebeck.de

***Abstract*—Exploration of natural and artificial underwater structures is an actual field in development and research projects. Acoustic detection methods are well known and can be used to create seabed and subbottom profiles. The systems have limitations for detection of small objects, especially in presence of large acoustic reflectors. The detection of flat buried objects like unexploded ordnance (UXO) is very difficult with acoustic systems. This work presents a simple setup that utilizes three unfocused transceivers to detect small acoustic disturbances in presence of large acoustic reflectors. We suggest a differential ultrasonic receiver to eliminate equal signal components of two overlapping receivers to detect small objects. Furthermore, we present a differential single-receiver system and an evaluation of different algorithms for data visualization and compare with the frequently applied envelope in single receiver systems. It is possible to detect small objects with the diameter of $6\,\mathrm{mm}$ located in the water-sediment interface with the differential receiver setup.**

***Index Terms*—Underwater, Ultrasonic, Obstacle Detection, Cable Detection, Subbottom**

I. Introduction

Acoustic imaging methods are well known and typically achieve a resolution of decimeters in underwater measurement systems [1] [2]. There are techniques available to detect small objects buried in sediments, like the 3D chirp system [1]. However, object detection in domains with strong reflected signals is not addressed yet.

The case study from Vardy et al. [3] demonstrates the detection with a 3D chirp system of objects, with a minimum surface of $0.3\,\mathrm{m} \times 0.3\,\mathrm{m}$. The objects detected by Vardy et al. [3] were buried in thin veneer above a flat bedrock surface with high acoustic contrast. A detection of smaller objects or above surfaces with different acoustic contrast is questionable from the results presented in [3]. Acoustic detection of buried UXO, where sediment and object reflections are separated are presented by Bucaro et al. [4] and Kargl et al. [5] for example.

The detection of objects that are located in the feedback of a surrounding with high acoustic contrast will be shown in this work. With a differential receiver setup we show the detection of small objects with a size of ~$\lambda/2$ ($6\,\mathrm{mm}$ diameter object at $f_0 = 125\,\mathrm{kHz}$), where the object reflection overlaps with the surrounding reflection.

Differential ultrasonic imaging is a common technique in medical monitoring applications, such as the imaging of induced lesions [6] [7] or intravascular imaging of microbubble contrast agents to track neovascularization [8]. The differential image is calculated on the basis of a reference image taken before the procedure. When detecting objects in underwater survey applications, it is not possible to obtain an image of the environment without the object. To solve this problem, we apply two receivers with partially overlapping beams to detect differences in the non-overlapping areas of both. Another approach is to use signals from consecutive measurements of a single receiver to calculate the differential images. The use of a locally offset reference image for difference image calculation requires homogeneous acoustic reflection properties of the environment.

We present the theory of our differential approach first and depict the theoretic pattern how an object appear. Subsequently we describe the implementation of the measurement setup, that is followed by the signal processing algorithms. At the end we present the results of the evaluation measurements in an artificial and natural like environment.

II. Approach

To measure small disturbances at large homogeneous reflectors, two receivers will be applied as shown in Figure 1. In absence of acoustic disturbing objects and structures the received signals of both receivers will be equal, assuming a symmetric stimulation. Asymmetric local disturbances (shown in Figure 1b) will result in different received signals. Hence,

Global Oceans 2020: Singapore - U.S. Gulf Coast

the amplitude difference of two received signals will be zero for homogeneous structures above and will increase with the presence of small objects or local changes in acoustic properties.

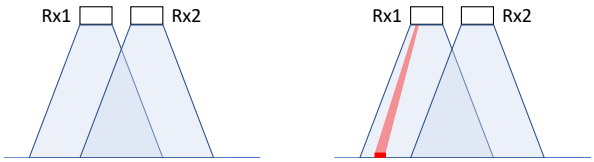

(a) Homogeneous reflector (b) Disturbed reflector

Fig. 1. Principle of differential receiving

The setup shown in Figure 1 is used to detect inhomogeneities in the non-overlapping areas of both receivers. If the system is moved across an object in front of a homogeneous reflector (from right to left), the object appears twice. Firstly, when the non-overlapping detection area of receiver 1 is reached and after passing the overlapping of both detection areas. Due to the differential measurement setup, objects in the overlapping areas are not recognized. This resulting pattern to identify the presence of an object depends on beam angle α, distance between the receivers d_{rcv} and the distance to the reflector d_{seabed}. As described in Section III, the size of each non-overlapping area is d_{rcv} and $r - d_{\mathrm{rcv}}$ for the overlapping area.

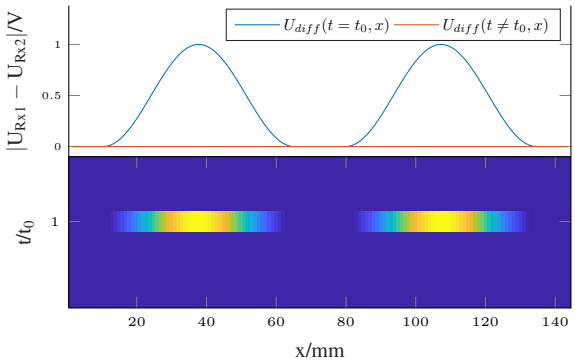

Fig. 2. Theoretic Pattern of an object crossed by differential measurement system in x direction

Figure 2 shows the expected pattern in theory when the differential setup crosses an object in the direction of x. The object appears with two hot sections and a cold section in the middle.

III. Implementation

Since this approach is based on a symmetric measurement arrangement and is sensitive regarding minor geometrical deviations, a mounting system for the transducers has been developed (see Figure 3). The mounting system is shown in Figure 5 (E).

To enable a flexible measurement setup, it provides three different positions for a transmitter (Tx) and four symmetrical pairs of positions for two receivers (Rx). The increment between the positions is 18 mm each. For the application we need waterproof transducers that generate strong acoustic signals.

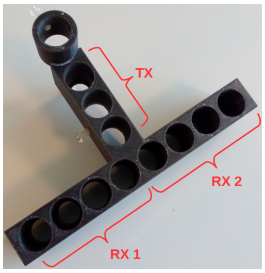

Fig. 3. Mounting system for differential measurement

The chosen UTR-1440-TT-R (from pui audio) fulfills these requirements with a 70° width conical beam.

A function generator (AFG300C from Tektronix) synthesizes a pulse for transmission with a center frequency of $f_0 = 125\,\mathrm{kHz}$, a bandwidth of $B = 70\,\mathrm{kHz}$ and an amplitude of $A = 1\,\mathrm{V}$. The voltage signal is amplified with a gain of $G = 10$ via an operational amplifier (OPA2134 from Texas Instruments), which output is connected to the ultrasonic transmitter. The signals of both the receiving transducers are filtered by an analog high-pass (order 1, $f_c = 16\,\mathrm{Hz}$). Afterwards, the combination of a non-inverting operational amplifier circuit (OPA2134 from Texas instruments, $G = 50$) and a programmable gain amplifier (AD8250 from Analog Devices, $G = 10$) pre-processes the measured signals before digitization with a digital oscilloscope (HDO 6054 from Teledyne LeCroy). A picture of the printed circuit board, which interfaces the signal generator, the transceivers, and the oscilloscope is shown in Figure 4.

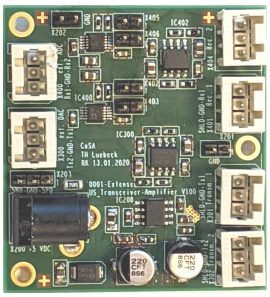

Fig. 4. Printed circuit board for analog signal processing

Measurements of this setup were performed in a glass aquarium. The outer dimensions of it are (LxWxH) 800 mm x 600 mm x 800 mm with 8 mm thickness. The bottom of our aquarium is filled with sand of grain size between 0.1 mm up to 2 mm (see A in Figure 5). The sediment height is ~100 mm. On top of the sediment we placed an acoustic foam plate (see B in Figure 5) and to get a homogeneous flat reflecting surface an acrylic plate 500 mm x 760 mm x 5 mm was placed on top of it (see C in Figure 5).

The measurements were performed with an automated XY-table that was constructed for measurements in the laboratory aquarium to move distinct sensor systems reproducible through the aquarium. With a resolution of 100 μm the table fulfills the requirement to move to positions with 1 mm distance. The

Global Oceans 2020: Singapore - U.S. Gulf Coast

mounting system with our transducers was adjusted at the XY-table and the vertical position in direction of z was adjusted manually (between green arrows in Figure 5). Both receivers are $54\,\mathrm{mm}$ away from each other (second position in the mounting system) and the transmitter is centered with an equal distance of $36\,\mathrm{mm}$ to both receivers. The angle α of aperture of all of the transducers is $70°$. D in Figure 5 refers to our test object which we tried to detect. Its orientation was chosen so that it is crossed by the receivers in transverse direction.

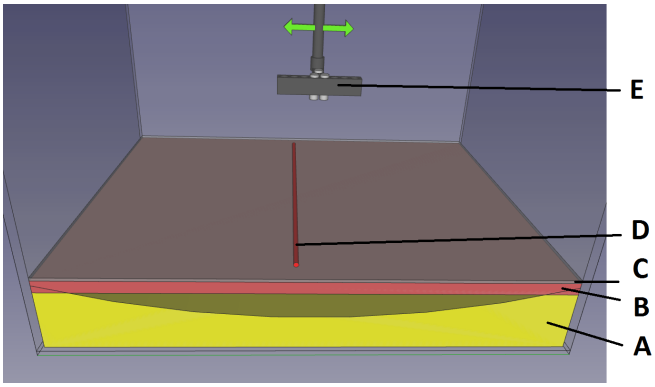

Fig. 5. Principle of Measurements

The distance between the receivers d_{rcv} and from the receivers to the seabed d_{seabed} are chosen by the calculation of the beam radius r in Equation 1 and the size of the object to be detected. Equation 1 can be derived from the beam geometry and a right angled triangle (see Figure 6).

$$r = d_{\mathrm{seabed}} \cdot tan(\frac{\alpha}{2}) \tag{1}$$

For the detection of a copper wire with $6\,\mathrm{mm}$ diameter we choose a beam radius $r = 50\,\mathrm{mm}$. With a beam angle $\alpha = 70°$ we calculate a distance to seabed of $d_{\mathrm{seabed}} \approx 71\,\mathrm{mm}$ with Equation 1. The distance between the receivers d_{rcv} can be interpreted as a shift of the center of the circular receiver areas. For the measurement we choose the second position for the receivers in our mounting system, where $d_{\mathrm{rcv}} = 49\,\mathrm{mm}$. Then the overlapping of both receivers is almost directly beyond them and the non-overlapping areas are left and right. Inhomogeneities are well detectable in the non-overlapping areas and will become undetectable in the center of the overlapping area, caused by the symmetry (see Figure 6).

For differential ultrasonic measurements, the signal of one receiver is considered as a reference. Therefore, the receivers are arranged in local relation and with a certain overlap to reduce the influence of environmental inhomogeneities in the reference and to amplify the artificial inhomogeneities.

IV. Signal Processing

We analyzed the received signals with different methods to compare them for visualization of small reflecting objects in differential signals. Firstly the signals are analyzed by the calculation of the envelope with a Hilbert Transformation.

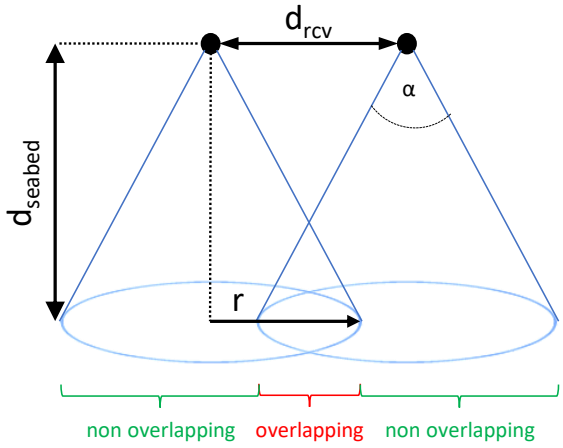

Fig. 6. Beam radius and overlapping in differential setup

Furthermore, the signals are also analyzed in frequency domain with a sliding Discrete Fourier Transformation (sDFT) and cross correlation with the transmitted pulse.

A. Preprocessing

The magnitude and phase of the received signals of both transducers in the same measuring position are not the same due to limitations in the alignment of the mounting system and different manufacturing tolerances of the sensors. Therefore, a preprocessing of the signals is performed to correct the phase and magnitude of the measurements.

B. Hilbert Transformation

The calculation of the envelope function is often used to visualize a received reflected pulse. A quadrature filter is useful to construct the envelope of a time function. The Z Transform of the real data series $X(Z)$ and the output $Y(Z) = Q(Z)X(Z)$ of a quadrature filter, denoted by $Q(Z)$, are used to calculate the envelope with Equation 2. [9]

$$e_t = \sqrt{x_t^2 + y_t^2} \tag{2}$$

The resulting curve envelopes the received signal, where the amplitude characterizes the reflective properties of the boundary layer. The distance $d_{reflector}$ to a reflector is calculated from the velocity of the sound c_{medium} and displacement time τ_{max} of local maximums as shown in Equation 3.

$$d_{reflector} = \frac{c_{medium} \cdot \tau_{max}}{2} \tag{3}$$

C. Sliding Discrete Fourier Transformation (sDFT)

As second approach to visualize small reflectors in the received signals, we apply a sDFT that performs Fast Fourier Transformations on small shifted segments through the received signal. Our implementation is based on the sDFT described by Jacobson [10]. We use a Hanning window containing $N = 53$ samples to extract the short time frames. It is adjusted to the spectral properties of the transmitted pulse with a center

Global Oceans 2020: Singapore - U.S. Gulf Coast

frequency of $f_0 = 125\,\mathrm{kHz}$, bandwidth $B = 70\,\mathrm{kHz}$ and the sample frequency of $f_s = 5\,\mathrm{MHz}$. To reduce artifacts and smooth the visualization the window shift size is set to $\Delta s = \frac{N}{2}$ (window overlapping is $50\,\%$). Then the computed spectrum of the window is correlated to the spectrum of the transmitted pulse $S_{Rx,Tx}(\tau) = (S_{Rx} \star S_{Tx})(\tau)$ and the window is rated with the correlated value $S_{Rx,Tx}(0)$.

D. Cross Correlation

The cross correlation of two time signals x and y provides the similarity of signal x and y at time τ, when signal y is delayed by τ [9]. To visualize reflections of the transmitted pulse we calculate a cross correlation between the transmitted pulse as y and the receiver signal as x (see Equation 4).

$$R_{xy}(\tau) = (x \star y)(\tau) = \begin{cases} \frac{1}{N} \sum_{n=0}^{N-m-n} x(n)y(n+\tau) & m \geqslant 0 \\ \frac{1}{N} \sum_{n=-m}^{N-1} x(n)y(n+\tau) & m < 0 \end{cases} \tag{4}$$

To smooth the resulting curve we performed a Hilbert transformation on the correlated signal.

E. Differential Signal

Initially the Hilbert Transformation described in Section IV-B is performed to both receiver signals. We use these results as a benchmark to evaluate the additional visualization of small objects with differential signals.

To detect small objects in front of big homogeneous reflectors, we calculate two types of differential signals $\Delta R_{1,2}$ and ΔR_{1t}. The first differential signal $\Delta R_{1,2}$ calculates the difference between both synchronized receivers Equation 5. The displacement d_{rcv} of the receivers in x-direction is $49\,\mathrm{mm}$.

$$\Delta R_{1,2} = R_1 - R_2 \tag{5}$$

The second differential signal ΔR_{1t} is calculated on two subsequent signals in a single receiver. ΔR_{1t} is the difference between a measurement taken by sending and receiving a pulse $R_a(t)$ in position *a* and subtract the result from a measurement $R_b(t)$ taken in position *b* (see Equation 6). The measurements in this work were performed, that the displacement between the positions *a* and *b* is $1\,\mathrm{mm}$. Therefore the single receiver system works with only $1\,\mathrm{mm}$ non-overlapping and $48\,\mathrm{mm}$ overlapping.

$$\Delta R_{1t} = R_a - R_b \tag{6}$$

Both differential signals are processed with the transformations described in Section IV-B - Section IV-C in order to them with regard to additional visualizable information.

V. Evaluation

Differential ultrasonic measurements provide an additional method to detect small objects in presence of big homogeneous acoustic reflectors. We present the detection of a small object, which is difficult to be detected and localized precisely in a Hilbert transformed signal of the received signal, with the differential approach.

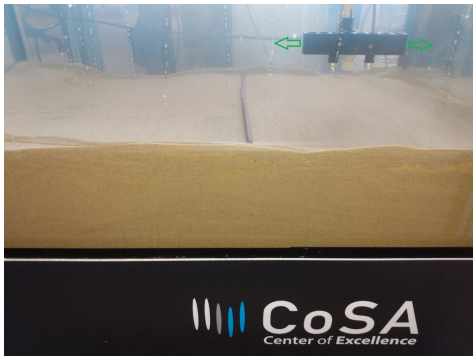

Fig. 7. Measurement of a copper cylinder laying on the sediment

The measurements were performed in a laboratory aquarium with two types of environment. They were carried out in an artificial environment, with the small objects placed on an acrylic plate, which is a homogeneous reflector, first and then placed on an acoustic foam plate.

Limitations of the differential measurement approach will be investigated on the basis of measurements of small objects on sandy sediment, which can be described as inhomogeneous natural environment. All measurements were performed with transmitter in the first position and both receivers in the second position in the mounting system symmetrically to the transmitter.

The processed results are visualized as 2D-Heatmap, with the relative slider position x on the abscissa and vertical distance z on the ordinate, which is calculated using the velocity of sound in water $c_{water} = 1480\,\frac{\mathrm{m}}{\mathrm{s}}$ and half of the time when signal is received. The measurements were performed with an automated XY-table that moved over $400\,\mathrm{mm}$ in steps of $1\,\mathrm{mm}$ in the aquarium across the object.

To evaluate received signals and the differential signals, the envelope of a single receiver are shown in the first row (a and e) and both differential approaches are shown per column (Figure 8 for example). The differential single receiver approach (see Equation 6) in the first column (b, c and d) and the differential dual receiver approach (see Equation 5) in the second column (f, g and h). On the differential approaches we performed the transformations described in Section IV-B - Section IV-C and visualized them per row.

Top to down comparison of the plots in a column allows the evaluation of one of both differential approaches against direct single transducer measurement (compare with a) and against the other transformation methods (compare b, c and d).

Comparison per row allows the evaluation of both different approaches against each other with same transformation algorithm performed (compare b with f, c with g, d with h).

A. Acrylic Plate Environment Measurements

As comparable reference measurement we use the results acquired in absence of any object at the acrylic plate in Figure 8.

Global Oceans 2020: Singapore - U.S. Gulf Coast

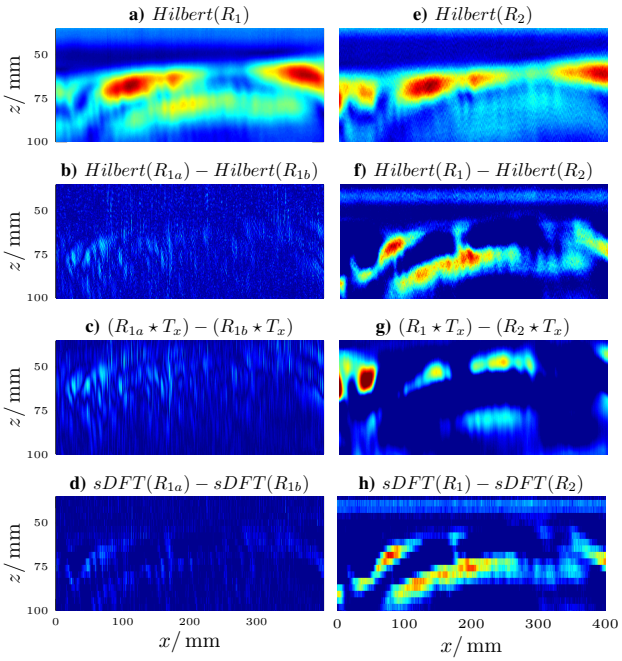

Fig. 8. Acoustic profiles of an acrylic plate.

The homogeneous reflecting plate results in a strong signal in a distance of ~60 mm in Figure 8a and e. Direct measured and Hilbert transformed data showing a well homogeneous reflection over x.

The single receiver differential approach (in Figure 8b, c and d) shows almost no signal, as expected, when no inhomogeneity is present. The dual receiver differential approach (in Figure 8f, g and h) indicate some inhomogeneities, that we can assign to reflections from unevenness of the sediment beyond the acrylic plate. Caused by the distance of 49 mm between both receivers, these inhomogeneities are visualized in the two receiver differential setup.

Figure 9 shows the results of the measurement of the acrylic plate with a long copper cylinder with 6 mm placed on it along the y axis at $x \approx 260\,\mathrm{mm}$.

The copper cylinder is well recognizable in the differential single transducer measurement Figure 9b, where the pattern of the object shows a typical cold (blue) region in the center position of the object, because its symmetric position leads to a differential signal with low magnitude. Comparing Figure 8a and Figure 9a the small copper cylinder is also detectable at $x \approx 250\,\mathrm{mm}$. Usually a reference image (like Figure 8a) without the object to be detected is not available in real exploration situations and a detection of our small object in Figure 9a only is not possible. However, the single receiver differential approach depicts the object with a very clear pattern (cold blue zone in the center, surrounded by hot zones, at $x \approx 230\,\mathrm{mm}$) in Figure 9b.

Because of the sediments unevenness depicted in Figure 8g it is not possible to recognize the small copper cylinder in Figure 9c with the dual receiver approach well. However, by adaption of the receivers distance d_{rcv} in the dual receiver

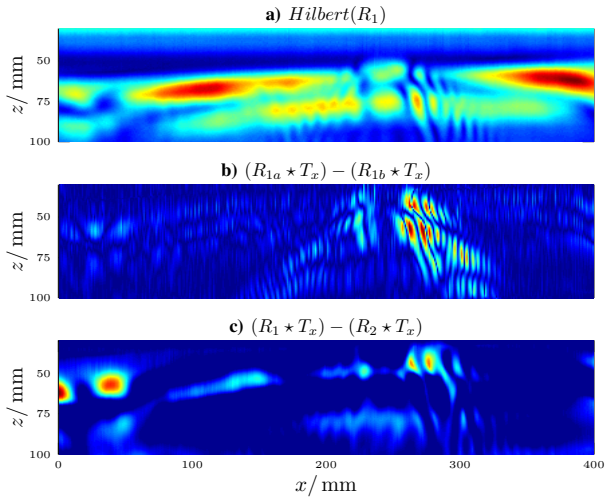

Fig. 9. Acoustic profiles of a copper cylinder (6 mm diameter) on an acrylic plate.

setup, this setup is able to be adapted to expected environment inhomogeneities and object sizes. The following measurement of the same small object in front of an absorber plate shows, that the dual receiver setup is also able to depict the object very clear.

B. Acoustic Foam Plate Environment Measurements

We performed our measurements in a second artificial environment applying an acoustic foam plate as big homogenoeous reflector. In Figure 10 the results for a measurement with the copper cylinder of 6 mm diameter placed at $x \approx 220\,\mathrm{mm}$, with adapted distance to the acoustic foam plate $d_{\mathrm{seabed}} \approx 160\,\mathrm{mm}$ and $d_{\mathrm{rcv}} = 18\,\mathrm{mm}$ is depicted. The reflection of the acoustic foam plate in Figure 10a provides a better main reflection regarding the homogeneity, compared to the acrylic plate in Figure 8a.

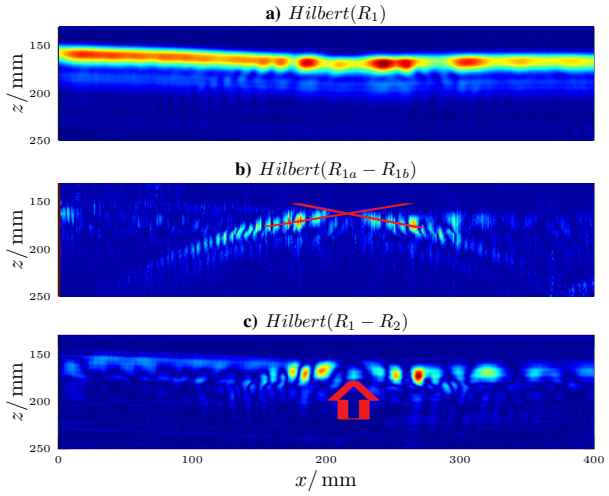

Fig. 10. Acoustic profiles of a copper cylinder (6 mm diameter) on an absorber plate.

Global Oceans 2020: Singapore - U.S. Gulf Coast

The position of the copper wire, placed at $x \approx 220\,\mathrm{mm}$, is recognizable with the measurements shown in Figure 10b and c. Figure 10b shows the point of intersection between the rising and falling digonals. This allows a very precise determination of the object position (cutpoint is at $x = 216\,\mathrm{mm}$), which cannot be determined precisely in Figure 10a. The center of the symmetrical reflection pattern in the measurement with two differential transducers, which is marked by the red arrow in Figure 10b, also allows the position to be determined (arrowhead is at $x = 221\,\mathrm{mm}$). The detection and precise localization of the copper cylinder placed on the acoustic foam plate with non-differential Hilbert transform in Figure 10a is very difficult and shows the advantages, that are additionally provided by the differential approach.

C. Sandy Sediment Environment Measurements

To evaluate the limitations and benefits for subsea exploration purposes like UXO detection, or cable tracking systems, we performed measurements with small objects placed on sandy sediment (see Figure 7) and buried objects in sandy sediment.

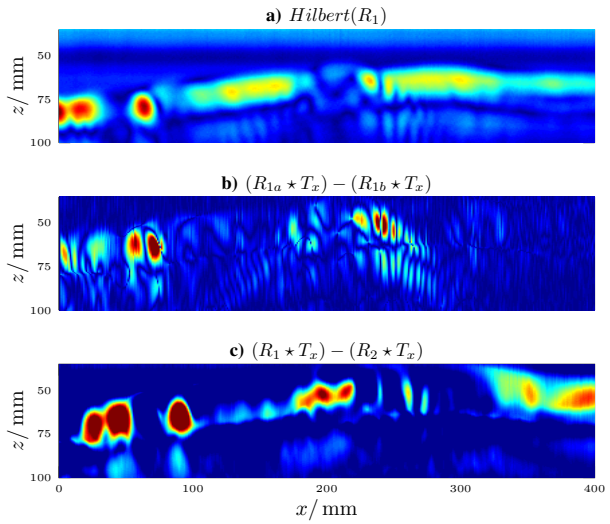

Fig. 11. Acoustic profiles of a copper cylinder (6 mm diameter) on a sandy sediment layer at $x \approx 210\,\mathrm{mm}$.

Figure 11 shows the results of the measurement, where the $6\,\mathrm{mm}$ diameter copper cylinder is placed at $x \approx 210\,\mathrm{mm}$. The pattern of the copper cylinder in the artificial environment can be found for the single transducer differential approach in Figure 11b and for the dual transducer differential approach in Figure 11c at the position, where the copper cylinder was placed.

Figure 11b also shows a significant inhomogeneity at $x \approx 75\,\mathrm{mm}$ that we expect as typical disturbances in a real environment, where the intensity of the ground reflection vary. But the pattern of the small copper cylinder in the single receiver differential setup in Figure 11b is recognizable again with a cold blue zone at $x \approx 210\,\mathrm{mm}$ surrounded by hot zones to the left and right. However, detection of small objects without prior knowledge of the object position in a nature like environment requires further research and system optimization for the dual receiver setup depicted in Figure 11c.

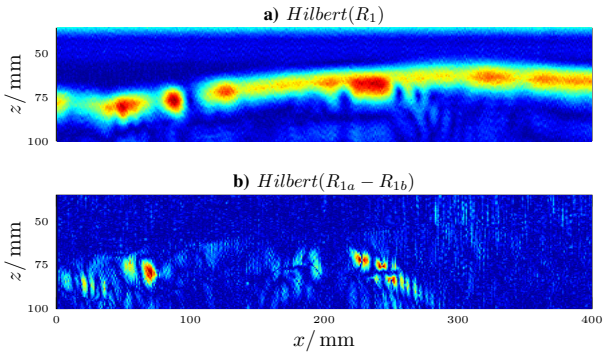

Fig. 12. Acoustic profiles of a copper cylinder (6 mm diameter) buried in sandy sediment at $x \approx 210\,\mathrm{mm}$.

Figure 12 shows the results, where the copper cylinder was buried ~$5\,\mathrm{mm}$ in the sediment. The filled trench of the object appears as hot zone at $x \approx 220\,\mathrm{mm}$ in the signal of the single receiver, but the object itself wouldn't be easy to be detected in Figure 12a. In Figure 12b the pattern of the object, even if it's buried, is recognizable at $x = 210\,\mathrm{mm}$, with the cold blue zone surrounded by two hot zones at the left and right.

VI. Conclusion and Future Work

Acoustic detection of small objects in presence of big reflectors, like the seafloor, is demonstrated in this work. With the implementation of a differential measurement system we detect small objects with better contrast compared to a single transducer setup with the visualization of the envelope. We showed the typical pattern for the appearance of objects in differential measurements and evaluated it with the measurements in a laboratory aquarium. At the end we were able to localize an object (copper cylinder with $6\,\mathrm{mm}$ diameter) buried in the sediment. The object size was ~$\lambda/2$ and the object was also detectable with overlapping reflections of the surrounding environment. To detect UXO in the sediment-water interface we plan a differential transducer setup with increased distance to the seabed of $d_{\mathrm{seabed}} \approx 5\,\mathrm{m}$ and a receiver distance of $d_{\mathrm{rcv}} \approx 0,5\,\mathrm{m}$ (refer Section III). With our single transducer differential measurements we presented an algorithm, that is adaptable to visualize signals of actual sensor systems, like altimeters or subbottom profilers.

Compared to the sDFT, the correlation and envelope calculation provide comparable results regarding visualization, with reduced computational effort and are therefore preferable. The pattern of the single receiver differential system can also be better recognized compared to the dual receiver system. Nevertheless, the dual receiver system with the fixed receiver spacing is advantageous when the system will be moved continuously in real applications because the overlapping and non-overlapping of the receivers is well known and independent to the speed of movement. However, the effort required to calibrate a dual-receiver system is higher (refer Section IV-A) than for a differential single-receiver system.

Since we expect higher inhomogeneities in real underwater applications, we will investigate our system in future with varying beam forming, distance and overlapping. With pattern detection as a basis, we plan an automatic detection of the shape of the object.

ACKNOWLEDGMENTS

This publication is a result of the research of the Center of Excellence CoSA and funded by the Federal Ministry of Economic Affairs and Energy of the Federal Republic of Germany (Id 03SX467B, Project EXTENSE, Project Management Agency: Jülich PTJ). Horst Hellbrück is adjunct professor at the Institute of Telematics of University of Lübeck.

REFERENCES

[1] M. Gutowski, J. M. Bull, J. K. Dix, T. J. Henstock, P. Hogarth, T. Hiller, T. G. Leighton, and P. R. White, "3d high-resolution acoustic imaging of the sub-seabed," *Applied Acoustics*, vol. 69, no. 3, pp. 262–271, 2008.

[2] J. S. von Deimling, P. Held, P. Feldens, and D. Wilken, "Effects of using inclined parametric echosounding on sub-bottom acoustic imaging and advances in buried object detection," *Geo-Marine Letters*, vol. 36, no. 2, pp. 113–119, 2016.

[3] M. E. Vardy, J. K. Dix, T. J. Henstock, J. M. Bull, and M. Gutowski, "Decimeter-resolution 3d seismic volume in shallow water: a case study in small-object detection," *Geophysics*, vol. 73, no. 2, pp. B33–B40, 2008.

[4] J. Bucaro, A. Sarkissian, B. Houston, H. Simpson, Z. Waters, D. Amon, K. Jig, S. Liskey, and T. Yoder, "Structural acoustic uxo detection and identification in marine environments–final report to serdp mr-2103," 2014.

[5] S. G. Kargl, K. L. Williams, T. M. Marston, J. L. Kennedy, and J. L. Lopes, "Acoustic response of unexploded ordnance (uxo) and cylindrical targets," in *OCEANS 2010 MTS/IEEE SEATTLE*. IEEE, 2010, pp. 1–5.

[6] H. Zhong, M.-X. Wan, Y.-F. Jiang, and S.-P. Wang, "Monitoring imaging of lesions induced by high intensity focused ultrasound based on differential ultrasonic attenuation and integrated backscatter estimation," *Ultrasound in medicine & biology*, vol. 33, no. 1, pp. 82–94, 2007.

[7] M. Ribault, J. Chapelon, D. Cathignol, and A. Gelet, "Differential attenuation imaging for the characterization of high intensity focused ultrasound lesions," *Ultrasonic imaging*, vol. 20, no. 3, pp. 160–177, 1998.

[8] M. Vavuranakis, I. A. Kakadiaris, S. M. O'Malley, T. G. Papaioannou, E. A. Sanidas, M. Naghavi, S. Carlier, D. Tousoulis, and C. Stefanadis, "A new method for assessment of plaque vulnerability based on vasa vasorum imaging, by using contrast-enhanced intravascular ultrasound and differential image analysis," *International journal of cardiology*, vol. 130, no. 1, pp. 23–29, 2008.

[9] J. F. Claerbout, *Fundamentals of geophysical data processing*. Citeseer, 1985.

[10] E. Jacobsen and R. Lyons, "The sliding dft," *IEEE Signal Processing Magazine*, vol. 20, no. 2, pp. 74–80, 2003.